Engineering and Technology Journal e-ISSN: 2456-3358

Volume 11 Issue 06 June-2026, Page No.- 10641- 10650

DOI: 10.47191/etj/v11i06.40, I.F. – 8.595

Simplified Approach to Design and Calibrate Cable-Stayed Structure Models

Danilo de Santana Nunes[1], José Luis Vital de Brito[2], Graciela Nora Doz[2]

[1]State University of Santa Cruz, Department of Engineering and Computing, ZIP Code: 45662-900, Ilhéus, Brazil

[2]Univesity of Brasília, Department of Civil and Environmental Engineering, ZIP Code: 70910-900, Brasília, Brazil

ABSTRACT: This paper presents and evaluates simplified approaches to design and calibrate a cable-stayed structure model based on results obtained from applying output-only modal identification methods. The data were collected during dynamic tests using an alternative data acquisition system. The process identified at least four flexural mode shapes of the structure and stay cables. The dynamic properties were determined theoretically using a 3D finite element model composed of beam and catenary elements. The calibration of the model was based on simplified sensitivity analysis and allowed the dynamic properties to be adjusted to the experimental values. The procedure provided an accurate updated model, with percentage of variation in the frequency varying from 0.00% for the first identified natural frequency to a maximum of 2.52%. The numerical model also provided good correlation between the mode shapes; the lowest Modal Assurance Criterion value was 0.9373, and might be used as reference in structural assessments.

KEYWORDS: Cable-Stayed Structure, Numerical Model, Dynamic Tests, Modal Identification, Updated Model.

I. INTRODUCTION

Cable-stayed structures are prominent worldwide. There has been a remarkable increase in special civil construction projects using this structural solution, whose basic premise is to support the deck with almost-straight cables, known as stay cables or stays. However, these structures may present service problems, raising concerns regarding the structure slenderness and catenary of the cables. Additionally, deferred (concrete shrinkage and creep and steel relaxation) and immediate (cable anchorage and immediate concrete deformation due to the effect of cable pre-tensioning) losses in the components may change the initial equilibrium scheme of the structure, thus increasing stresses and safety problems of the structure under normal use.

In general, the structural performance of civil engineering infrastructure decreases over time because of immediate or short-term factors after or during construction period, such as inappropriate curing, vibration, shrinkage cracks, and workmanship, and long-term effects, such as material degradation and weathering, rebar corrosion, water seepage, loading conditions, environmental degradation, and crack formation (Mishra et al. 2022). In this way, the Structural Health Monitoring (SHM) is an important guarantee for the safe operation of the structure and has always been a research hotspot in the field of civil engineering. The modern monitoring system integrates functions such as data collection, using real-time monitoring of response by installing sensors in various parts of the structure, health diagnosis, and damage warning, making the entire structural testing process dynamic and convenient (Deng et al. 2023). As important links in the transport infrastructure system, cable-stayed structures (bridges, viaducts and footbridges) are among the most popular candidates for implementing SHM technology. With existing bridge infrastructure now maturing in many countries, and the addition of new structures every year, the ability to proactively and cost effectively monitor their condition for strategic planning of maintenance, rehabilitation, and repair activities is becoming increasingly important (Sharry et al., 2022). There are increasing demands on existing infrastructure with respect to traffic loads and intensity. Many highway and railway bridges are still in use despite that they are approaching or have exceeded their original design life. Lifetime extension is the preferred option to ensure continuous operation (Svendsen et al., 2021). To highlight the benefits of implementing SHM, Güemes et al. (2020) illustrate the degradation process experienced in service for every structure/mechanical system. By improving the material's properties, and particularly the material's toughness, the slope of the presented curve is decreased and the durability of the structure is increased. Besides acquisition costs, the second main factor that influences life cycle costs is related to the maintenance or actions needed to keep and recover the structure within a satisfactory state, after incipient damages.

Many uncertainties related to ageing, deterioration and damage accumulation are present in the structures and, consequently, to existing structures that are approaching or have exceeded their original design life. Thus, considering the requirements for precise numerical models in lifetime extension analyses, entire process should be carried out using validated models that can be effectively established and adequately represent the current state given these inherent uncertainties (Svendsen et al., 2021). In fact, the analyses generally involve accurate numerical modelling of the structure by using the Finite Element Method (FEM), which is a powerful tool for structural analysis. However, the numerical model of a structure is established based on highly idealized engineering drawings and designs that may not truly represent all aspects of the structure. Significant discrepancies may exist between the characteristics predicted by FEM and those measured from a structure (Wu and Li 2004). A structural Model Updating (MU) is necessary, in which experimental results are used to refine the mathematical model of a physical structure, resulting in updated matrices that can reproduce the measured structural modal properties (Ren and Chen 2010). Structural models that have been verified, refined, and tuned to actual measurements can reduce the uncertainties in SHM, and provides a good basis for management (Schlune et al. 2009; Cismaşiu et al. 2014). These numerical models can be calibrated in terms of the material parameters and boundary conditions and according to on-site responses to dynamic loads (Chisari et al. 2015). The dynamic properties are still useful for MU (Yuen 2012) and are a good tool for nondestructive damage assessment (Malekjafarian and Obrien 2014; Sun et al. 2020).

This research used a cable-stayed footbridge as study case. The modern trend toward building slender and lightweight footbridges is notorious (Tubino et al. 2016; Nimmen et al. 2016; Setareh and Gan 2018) and, despite having several modal test techniques available, these structures can be excited with high energies for the designed load, such as the crossing of people. Consequently, the response generated by pedestrians walking or jumping is widely used in the testing and dynamic analysis of footbridges (Bin et al. 2011; Setareh 2016; Feng et al. 2019; Brownjohn et al. 2016). Thus, the Ambient Vibration Test (AVT) and the Operational Modal Analysis (OMA) were used to identify the experimental dynamic properties required for the MU process.

An initial numerical model was designed to guide the experimental routine and, after performing the experimental tests and identifying the selected dynamic properties (natural frequencies and mode shapes), this model was updated. Several space frame models consisting of line elements to model cable-stayed structures have been offered by the literature. These models are distinguished from each other depending on how the deck has been modelled: single-girder, double-girder, triple-girder, or multi-scale. To analyse their dynamic behaviour, Finite Element (FE) models (beam elements, shell and solids objects) have been used for the tower and deck, and the numerical model denominated "spine" specifically for the deck, each with a certain degree of success. The stay cables have been simulated as usual truss elements, ignoring the nonlinear behaviour of stay cables due to sag, as modified truss elements, by considering the secondorder effects caused by their weight through an equivalent modulus of elasticity or multi-element cable system which divides each cable into several straight truss elements, and with "catenary" elements (cable elements) which directly accounting their deformed shapes due to the self-weight. One of the many challenges in the SHM process is to develop an initial FE model that can accurately reflect the dynamic characteristics and the overall behaviour of a structure; its accuracy in turn influences the accuracy of the final updated model (Yue and Li 2014; Zhu et al. 2014; Park et al. 2014; Asadollahi and Huang 2018; Sharry et al., 2022). Discrepancies inevitably exist between the computed numerical model results and the measured behaviour of the structure. MU process seeks to correct the initial FE model errors and has been widely applied to obtain an updated model that reflects the real behaviour of the structure. Finite element MU is a well-recognised approach for SHM purposes, as an accurate model serves as a baseline reference for damage detection and long-term monitoring efforts. MU can be described as an inverse problem, i.e., the process of calculating, from a set of observations, the required factors or parameters that produced these observations. The system matrices can be updated via direct, iterative, and stochastic methods, usually based on a preliminary sensitivity check of the updating parameters. The direct methods, commonly called manual tuning, is performed directly on the numerical model by the operator and aim to update the mass and stiffness matrices in a single step FE procedure. The iterative methods, also broadly referred to as automatic tuning or sensitivity-based updating, are generally formulated around the minimization of the differences between the measured behaviour and the model predictions (usually natural frequencies) in the form of an objective function. It uses sensitivity-based optimization to construct the final model so that changes to the updating parameters are also minimized by their inclusion in the objective function. Stochastic finite element MU methods generally utilize Bayes' theorem to estimate a posterior probability density function of the model parameters to be updated. Although stochastic updating methods present the advantage of taking uncertainty and data variability into account, its computational expense is very high compared to other methods. (Park et al. 2014; Benedettini and Gentile 2011; Bursi et al. 2014; Bedon et al. 2016, Sharry et al., 2022).

This study evaluated simpler approaches for designing and updating numerical models of cable-stayed structures. As a result, the presented approach reduces the required computational effort, in contrast to the current trend toward more refined models with automatic and stochastic update processes. First, an initial 3D FE model with 3D beam elements was designed for the footbridge based on the structural design drawings and field measurements. Subsequently, the translational and rotational springs were calculated and inserted considering the soil–structure iteration. This was followed by a sensitivity analysis to evaluate the change in the natural frequencies as a function of changing the material parameters to guide the direct MU process. Lastly, the selected material parameters were changed manually to enhance the correlation between the experimental and theoretical natural frequencies, and posterior validation was performed using the correlation between the experimental and theoretical mode shapes. All of the procedure steps described above were applied to a cablestayed footbridge.

II. MATERIALS AND METHODS

A. Structure Studied

The cable-stayed footbridge investigated in this study crosses the BR101 route at km 88 in the city of Nossa Senhora do Socorro, Sergipe/SE, Brazil. The deck is 58.0 m long and 2.0 m wide, and is divided into two parts by a single central tower that is 22.4 m tall. The semi-fan cable arrangement of the bridge is distributed spatially in two inclined planes on each side of the deck. Each plane contains 8 stay cables. Half of the 16 cables are backstays, anchored externally to a foundation block (see Figures 1 and 2). For all of the stays, 32-mm-diameter Dywidag bars were used, and the superstructure concrete has fck = 30 MPa (design value).

Fig. 1. Cable-stayed footbridge in Sergipe, Brazil

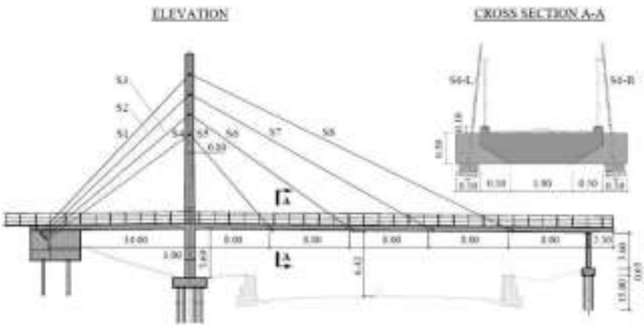

Fig. 2. Elevation and deck cross-section of the cable-stayed footbridge (units: m)

B. Experimental Routine

This study used the Arduino/Genuino 101 board, which has an approximate cost of \$40, in combination with Realterm software to capture and record the acceleration time series. The acceleration signals were measured using the on-board Bosch BMI160 3-axis accelerometer and gyroscope with ±2 g sensitivity at 16384 LSB/g and 180 μg/√Hz typical output noise. This alternative sensor was previously tested by the research team in three different laboratory models, in a specific frequency range corresponding to that of civil structures, such as cable-stayed structures. All the experiments were compared to professional accelerometers with promising results. More details regarding the proposed acquisition system can be found in Nunes et al. (2019). The acquisition system assembled to perform the dynamic tests of the complete structure consisted of a computer, three 5.0-mlong USB A/B cables, three 15.0-m-long USB A/B extension cables equipped with signal amplifiers, and three Arduino boards. For the stay cable tests, the acceleration time series were obtained using a single Arduino board, which was connected to the computer by a 3.0-m-long USB A/B cable. During the tests, the wind, air displacement due to trucks driving under the footbridge, and crossing of people were the main excitation factors observed. Additionally, for the global tests, two people ran and jumped along the footbridge deck to increase the excitation energy. For the stay cable tests, the excitation energy was increased by random displacements, both in direction and magnitude, manually imposed. Figure 3 shows the data acquisition system and the Arduino/Genuino 101 board detail.

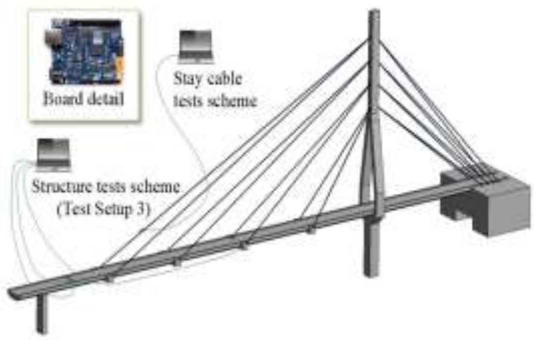

Fig. 3. Proposed data acquisition system installed on the footbridge (Test Setup 3 and stay cable tests)

The global tests used 17 setups along the deck and tower, with one board as a reference and two as mobile sensors. The reference sensor was positioned in the region of the connection between the S6 stay and the deck. The position was shown to be promising because significant coordinates were observed for almost all of the theoretical mode shapes provided by a preliminary numerical model of the footbridge. Details about the tests can be found in Nunes et al. (2023).

C. Dynamic identification methods

The vibration method was used to determine the stay cable forces. The Peak-Picking method (PP) was used to identify the necessary natural frequencies. For the complete structure, two output-only dynamic identification methods were used; the Curve-fit Frequency Domain Decomposition (CFDD) and the data-driven Stochastic Subspace Identification – Unweighted Principal Components (SSI-UPC). These methods are presented below.

1) Peak-Picking Method (PP):

In this method, the structure's natural frequencies are associated with the values of frequency peaks, where the amplitude tends to infinity in the Frequency Response Function (FRF) and in the power spectrum estimated using the Fast Fourier Transform (FFT). Equation 1 shows the FFT applied to the correlation functions R(τ) (auto and crossed), resulting in the power spectral density (PSD) functions S(f):

$$S(f)=\int_{-\infty}^{\infty} R(\tau)e^{-i2\pi f\tau}\,d\tau \tag{1}$$

For multiple degrees of freedom, the spectral information can be organized into matrices using the Equation 2:

$$S_q(f)=H(f)\,S_p(f)\,H^H(f) \tag{2}$$

Where $S_q(f)$ is the PSD functions matrix of response, H(f) is the FRFs matrix ("H" index means transposed conjugate of matrix), and $S_p(f)$ is the PSD functions matrix of excitation.

2) Curve-fit Frequency Domain Decomposition (CFDD):

The CFDD also uses the PSD functions of the response and adopts the following steps:

- Calculation of the normalized PSD functions of the response: Normalization is an artifice used to overcome certain drawbacks when working with several measurement points and test setups. This provides a higher number of frequency peaks of each auto-spectrum to be identified, and the variation in excitation intensity during the test, which leads to different energy contents for the measured time series. Thus, it is sought to normalize the energy content of each spectrum, which can be performed by dividing each ordinate of the $PSD_i(\omega)$ function by summation of all ordinates N, resulting in a normalized function $NPSD_i(\omega)$, as follows (Equation 3):

$$NPSD_i(\omega)=\frac{PSD_i(\omega)}{\sum_{k=1}^{N} PSD_i(\omega_k)} \quad (3)$$

- Calculation of the average $NPSD_i(\omega)$, the ANPSD functions, by Equation 4:

$$ANPSD=\frac{1}{setups}\sum_{i=1}^{setups} NPSD_i(\omega) \quad (4)$$

- Singular Value Decomposition (SVD) of the average normalized PSD functions matrix: The decomposition technique allows decoupling of the spectral density matrix. The matrix is decomposed into spectral density functions of each degree of freedom corresponding to each mode of vibration of the structure;
- Peak selection of the average normalized PSD decomposed in singular values, which correspond to the structure’s natural frequencies, and weighting of the singular vectors using the respective singular values to calculate their average values;
- Application of the inverse FFT to the spectral density functions to obtain the corresponding autocorrelation functions, which are used to estimate the natural frequencies and damping ratios, and elimination of the harmonic components using linear interpolation applied to the power spectrum related to the singular value under analysis, in general the first one;
- Application of the curve fitting algorithm: The optimization algorithm calculates the function parameters that result in the minimum error, i.e., it determines the curve that best fits the data of the average normalized PSD function decomposed into the first singular value;
- Evaluation of mode shapes through the singular vectors related to the singular values (natural frequencies) obtained at the degrees of freedom (measurement points). Details about the method can be found in Jacobsen and Andersen (2008) and Jacobsen et al. (2008).

3) Stochastic Subspace Identification – Unweighted Principal Components Method (SSI-UPC):

Subspace methods identify state-space models from (input and) output data by applying numerical techniques, such as QR factorization and SVD. The discrete-time deterministic state-space model is obtained by:

$$x_{k+1}=Ax_k+Bp_k$$
$$y_k=Cx_k+Dp_k \quad (5)$$

Where x_k is the discrete-time state vector, p_k are the input samples, y_k are the output samples, A is the discrete system state matrix, B is the discrete input matrix, C is the output matrix, and D is the direct transmission matrix.

The SSI-UPC follows these steps:

- Kalman filter application and organization of response time series by the Hankel matrix;
- Projection matrix weighting: The data matrices are weighted before the application of the SVD. This weighting determines the state-space basis in which the identified model will be identified. In SSI-UPC, as the term "unweighted" suggests, the weighting matrices W_1 and W_2 applied to the ref projection matrix P_i are equal to identity matrices with the same order, as follows:

$$P^{ref}_{i,w}=W_1P^{ref}_i W_2 \quad (6)$$

Where $P^{ref}_{i,w}$ is the weighted projection matrix, influencing the state vector prediction.

$$X_i=O^*_i P^{ref}_{i,w} \quad (7)$$

Where X_i is the optimal state vector prediction and O^*_i is the conjugate transpose of the observability matrix.

- SVD: The decomposition reveals the order of the system and the column space of the observability matrix O_i (from Eq. 7).
- Identification of system matrices: After applying the numerical techniques described above, the stochastic statespace model representation for multiple degrees of freedom results in:

$$\begin{pmatrix} X_{i+1} \\ Y_{i/i} \end{pmatrix} = \begin{pmatrix} A \\ C \end{pmatrix} X_i + \begin{pmatrix} W_i \\ V_i \end{pmatrix} \quad (8)$$

Where X_{i+1} is the Kalman filter state sequence, $Y_{i/I}$ is the Hankel matrix with only one block row, W_i is the process noise, and V_i is the measurement noise.

The measurement noise is considered as white noise and can be excluded from the process because of its constant energy content, resulting in Eq. 9:

$$\begin{pmatrix} A \\ C \end{pmatrix} = \begin{pmatrix} X_{i+1} \\ Y_{i/i} \end{pmatrix} X^*_i \quad (9)$$

Where X^*_i is the conjugate transpose of the X_i vector.

The modal parameters of the dynamical system can then be extracted from the state matrix A, which contains the matrices of the structure (M, C_1 and K), based on solving an eigenvalues and eigenvectors problem. Equation 10 shows the system matrices:

$$A = \begin{bmatrix} 0 & I \\ -M^{-1}K & -M^{-1}C_1 \end{bmatrix} \quad (10)$$

Where M is the mass matrix, C_1 is the damping matrix, and K is the stiffness matrix of the structure.

- Stabilization diagram: Selects stable, unstable and noise modes, thus determining the dimension of the ideal state space. For modes to be classified as stable they must meet certain requirements, e.g., valid range of damping rates. By adjusting this range, harmonic components and non-physical modes can be filtered out, with only true mode highlighted as stable modes.

Details about the method can be found in Peeters and De Roeck (1999), and Peeters (2000).

D. Numerical modelling and calibration

A 3D FE model of the footbridge was created for this study using SAP2000 software. Six-degree-of-freedom single beam elements at each end were used for the deck and tower, and cable elements (“catenary elements”) were used for the stay cables, totalling 349 beam elements, 16 cable elements, 468 nodes, and 2808 degrees of freedom. The various structural elements were designed as follows:

i) Deck – four 3D beam elements with equivalent stiffness were used. The cross-section was divided into four parts; the moment of inertia and the centroid showing the longitudinal equivalent element positions were calculated for each part. The stiffness of transverse elements was calculated for the 0.5 m half-widths between them (3D beam elements were also used). The boundary conditions between the deck and tower were considered fixed, whereas those between the deck and anchorage block were initially assumed to be fixed. The pylon support was initially assumed to be fixed for displacements only. Initially, the concrete weight per unit volume was assumed as 25.0 kN/m^3 and the modulus of elasticity as 30 GPa. Figure 4 shows the detail of the division of the crosssection into four parts. For each detached part, the inertia and centroid were calculated, defining the stiffness and transverse position of each longitudinal beam element (LBE).

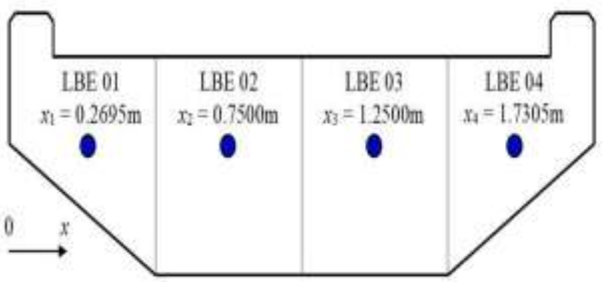

Fig. 4. Detail of the division of the deck cross-section to define the stiffness and positions of the longitudinal beam elements

As the difference was very small, the LBE distribution was homogenized. As a result, the LBE 01 and LBE 04 coordinates were changed to $x_1 = 0.2500$ m and $x_4 = 1.7500$ m, respectively, and the transverse distance between all of the longitudinal elements was 0.50 m. Inertia was calculated relative to the centroidal axes without these adjustments, resulting in a 0.50 × 0.50 m mesh for the deck.

ii) Tower – 3D beam elements considering the design cross-section were used. The boundary conditions between the tower and foundation were initially assumed to be fixed. Initially, the concrete weight per unit volume was assumed as 25.0 kN/m^3 and the modulus of elasticity was assumed as 30 GPa.

iii) Stay cables – “catenary elements” were used. They consider the nonlinearity caused by the deformed cable geometry due to the self-weight. The cable deformed shape and the axial forces measured on-site were added to the model through two tools implemented in SAP2000. The first tool calculates the cable geometry as a function of the force. The second, called “Target Force,” imposes the cable axial force for the selected load case, which was the self-weight load in this case. The weight per unit volume provided by the manufacturer was 76.9415 kN/m^3 and the initial modulus of elasticity was assumed as 205 GPa.

The natural frequencies of the cable were used to determine the on-site axial forces of the stays. A simple way to estimate the cable forces in terms of the natural vibration frequencies is to use the vibrating string Mersenne/Taylor law, given by Equation 11 for a cable pinned at both ends.

$$f_n = \frac{n}{2L}\sqrt{\frac{T}{m}} \tag{11}$$

Where L is the span length, T is the cable tension, m is the mass per unit cable length, and n is the mode shape number.

The cable length was obtained from the solid model, i.e., it is the length between the concrete element faces.

The MU process was performed through manual tuning. With this method, changes must be systematically made to the model details (e.g., the mesh configuration and element types), parameters describing the element geometry and materials (e.g., the mass, moments of inertia, and modulus of elasticity) (Daniell and Macdonald 2007), and the boundary conditions. The level of approximation can be measured by comparative indexes, such as percentage of variation in the frequency (FER index) and Modal Assurance Criterion (MAC index). The goal is to minimize the FER that represents the correlation between the natural frequencies and maximize the MAC. The MAC varies between 0 and 1, where a value of 1 indicates a complete correlation between the two mode shapes. Both indexes were used in this study.

III. RESULTS AND DISCUSSIONS

A. Stay cable dynamic identification

The natural frequencies of the cables were identified using the PP method, presented in previous section. This technique was applied using Matlab software. Figure 5 shows the acceleration time series recorded with the acquisition system in stay S6-R, for example (see Fig. 2 for nomenclature).

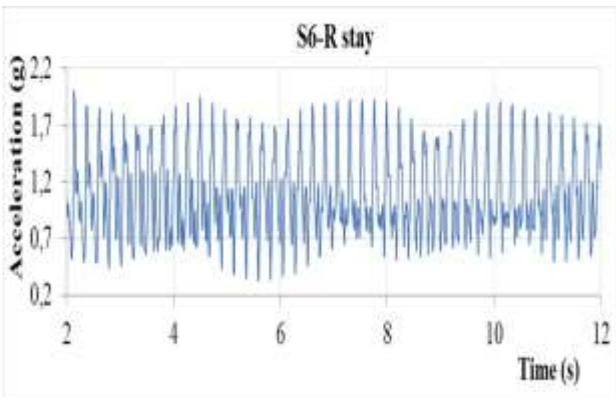

Fig. 5. Acceleration time series for stay S6-R

Figure 6 shows the PSDs of the signals shown in Fig. 5.

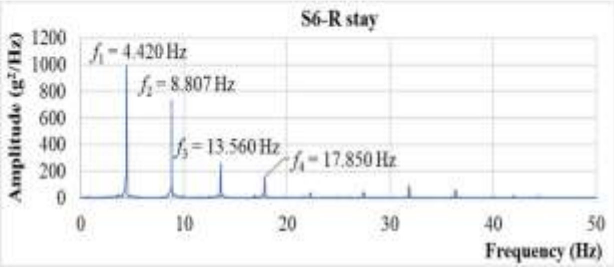

Fig. 6. PSDs of the acceleration signals measured for stay S6-R

Table I lists the stay cable axial forces related to the 1st, 2nd, 3rd, and 4th natural frequencies obtained for all stays using the PP method and the Mersenne/Taylor law, and the average force (T).

Table 1. Stay Cable Axial Forces Related to The First Four Identified Natural Frequencies

Stay cable	$T[f_1]$ (KN)	$T[f_2]$ (KN)	$T[f_3]$ (KN)	$T[f_4]$ (kN)	Average T (kN)
S1-R	266.19	281.82	269.81	284.78	275.65
S1-L	252.52	257.72	254.65	274.90	259.95
S2-R	203.40	210.35	204.37	222.53	210.16
S2-L	215.46	221.22	217.34	234.42	222.11
S3-R	178.06	173.41	179.66	187.57	179.67
S3-L	183.01	177.07	182.97	191.38	183.61
S4-R	156.37	168.43	165.69	170.88	165.34
S4-L	143.69	155.26	153.79	158.65	152.85
S5-R	95.43	97.27	100.13	103.76	99.15
S5-L	105.23	106.53	109.33	113.70	108.70
S6-R	173.21	171.92	181.13	176.55	175.70
S6-L	179.85	178.58	187.87	182.54	182.21
S7-R	174.95	182.48	174.99	179.75	178.04
S7-L	175.29	179.06	171.57	176.36	175.57
S8-R	226.94	226.85	238.03	231.02	230.71
S8-L	238.03	235.15	245.63	239.48	239.57

B. Dynamic Structural Identification

The dynamic properties were identified from AVT data using two output-only techniques, CFDD and SSI-UPC. Both methods are available in the Modal 4.0 ARTeMIS software used in this study. Figure 7 shows the acceleration time series captured in Test Setup 6, for example. Figure 8 shows the related PSD function decomposed into three singular values and the application of the curve-fitting algorithm to the 2nd and 4th peaks using the CFDD method.

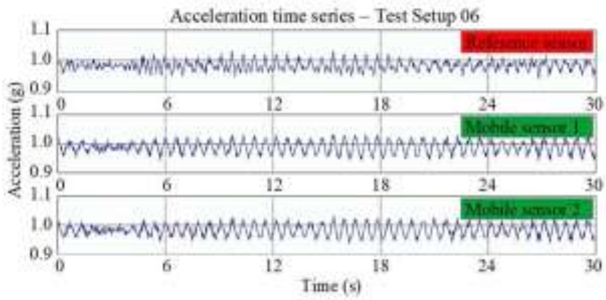

Fig. 7. Acceleration time series recorded in Test Setup 06(Reference sensor, Mobile sensors 1 and2)

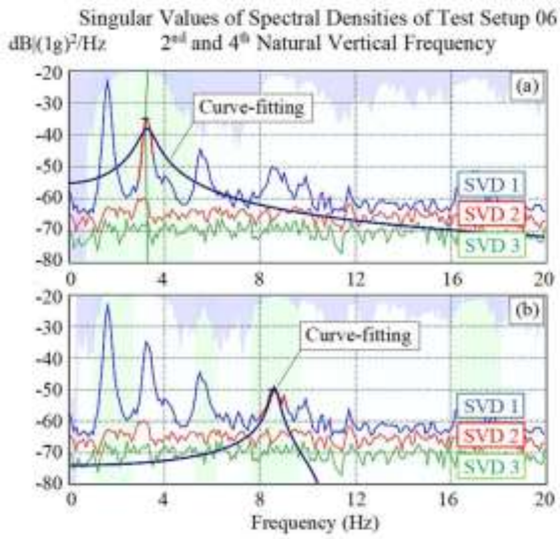

Fig. 8. Application of the curve-fitting algorithm to the (a) 2nd and (b) 4th peaks using the CFDD method

The curve-fitting algorithm adjusted three of the four peaks in the first singular value of the spectrum (see Table 2). If the first, second, and fourth frequencies were obtained only by selecting the spectrum peaks, the values would be 1.602, 3.203, and 8.508 Hz, respectively, whereas the third frequency has the same value with both methods. The method seems promising for power spectral densities obtained from noisy signals.

Figure 9 shows the stabilization diagram for the estimated state-space model resulting from the SSI-UPC method.

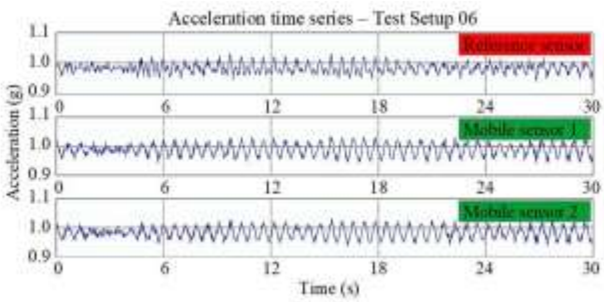

Fig. 9. Stabilization diagram for the estimated state-space model resulting from the SSI-UPC method

Both methods, the SSI-UPC and CFDD, identified and highlighted the same modes as stable. However, the SSI-UPC method indicated two unstable modes close to the first spectrum peak, probably resulting from the noisy signal.

Table 2 lists the first four natural frequencies identified by the CFDD and SSI-UPC methods.

Table 2. First Four Natural Frequencies Identified by The Cfdd and Ssi-Upc Methods

Flexural mode Shape	fCFDD (hz)	SSI-UPC (hz)	Difference (hz)
1st	1.617	1.611	0.006
2nd	3.288	3.276	0.012
3rd	5.505	5.638	0.133
4th	8.608	8.625	0.017

The two methods provided similar natural frequency values; the greatest difference of 0.133 Hz was observed for the third frequency. The results of the CFDD method were used in the MU process. The chosen was based on a qualitative analysis of the experimental mode shapes. Figure 10 shows the first four mode shapes identified by the CFDD method.

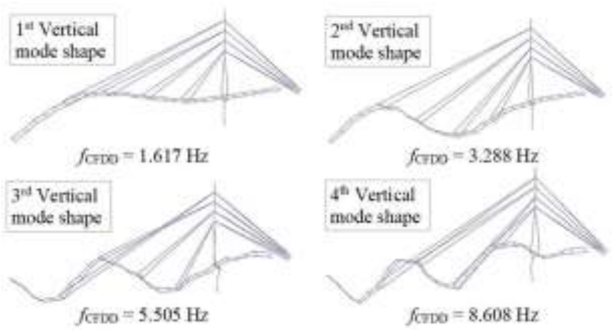

Fig. 10. First four identified mode shapes identified by the CFDD method

C. Numerical Model Calibration

Modal analysis of the initial model (Model 1) was performed to evaluate its proximity to the experimental model. The differences between the first four natural frequencies are listed in Table 3. Importantly, although linear, the performed modal analysis considered the footbridge deformed under the dead load. A nonlinear static analysis with SAP2000 allowed a load case to be created consisting of the self-weight and the experimental cable forces.

After observing that the first natural frequency was higher in the numerical model compared to the experimental model, altering the boundary conditions of Model 1 was the first change proposed. Thus, rotational springs of 2×10^8 kNm/rad were adopted to simulate the boundary conditions between the tower and the foundation, as well as that between the deck and the anchorage block. Based on the dimensions and stiffness of the support device (neoprene) and pylon, translational springs were calculated to simulate the boundary conditions between the deck and the pylon, resulting in transverse and longitudinal springs of 32.5×10^3 kN/m and 6.5×10^3 kN/m, respectively. Changes in the stiffness values of the rotational springs were tested. Because no significant effects on the natural frequencies were observed, the tower and anchorage block boundary conditions were not included in the update process. The adopted value was used until the final model. This may have occurred, for this case, due to the use of half of the cables as backstays, which limited the rotation of the mast. The implemented changes resulted in Model 2.

The final numerical model (Updated Model) was obtained by manually changing the Young's modulus of the concrete, concrete weight per unit volume (E_C and γ_C, respectively), and Young's modulus of the steel cable (E_S), which may vary by 5% (between 194.75 GPa and 215.25 GPa) according to the manufacturer. In this case, the selected parameters were the most important and promising for updating the model. A simplified sensitivity analysis was performed to evaluate the rate of change of the natural frequencies (from the first to the fourth flexural mode shapes) of Model 2 due to a +5% change in the structural parameters listed above. Figure 11 shows the sensitivity coefficients computed in the analysis.

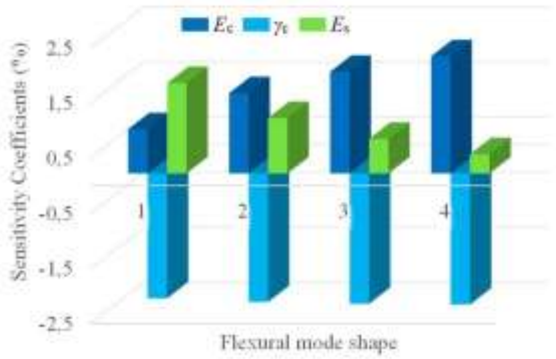

Fig. 11. Sensitivity coefficients of Model 2

The results show that changes in E_C have a greater effect on the higher-order flexural natural frequencies, while changes in E_S have a greater effect on the lower-order flexural natural frequencies. Furthermore, changes in γ_C affect all four first natural frequencies with a similar intensity. The manual updating process was performed in three steps. Because the first natural frequency was higher in Model 2 compared to the experimental model, Step 1 consisted of gradually decreasing E_S. Then, because the fourth natural frequency was lower in Model 2 compared to the experimental model, Step 2 consisted of increasing E_C. After these steps, the first natural frequency presented a value slightly higher than the experimental value, and thus Step 3 consisted of increasing γ_C. The approach resulted in E_C = 31.0 GPa, E_S = 198.5 GPa, and γ_C = 25.3 kN/m^3. Table 3 lists the results obtained from the systematic manual updating process.

Table 3. Steps of The Updating Process Applied To MODEL 2

Step 1 E_C=30 GPa γ_C=25 kN/m^3		E_S (GPa)			FER (%)
	205.0	200.0	195.0	198.5	
1st frequency (Hz)	1.635	1.622	1.608	1.618	0.06↑
2nd frequency (Hz)	3.242	3.226	3.210	3.221	2.04↓
3rd frequency (Hz)	5.447	5.430	5.413	5.425	1.45↓

4th frequency (Hz)	8.341	8.326	8.312	8.322	3.32↓
Step 2 E_S=198.5 GPa γ_C=25 kN/m³		E_C (GPa)			FER (%)
	30.0	30.5	31.0	-	
1st frequency (Hz)	1.618	1.622	1.626	-	0.56↑
2nd frequency (Hz)	3.221	3.237	3.253	-	1.06↓
3rd frequency (Hz)	5.425	5.459	5.492	-	0.24↓
4th frequency (Hz)	8.322	8.381	8.440	-	1.95↓
Step 3 E_C=31.0 GPa E_S=198.5 GPa		γ_C (GPa)			FER (%)
	25.0	25.1	25.2	25.3	
1st frequency (Hz)	1.626	1.623	1.620	1.617	0.00
2nd frequency (Hz)	3.253	3.246	3.240	3.234	1.64↓
3rd frequency (Hz)	5.492	5.481	5.471	5.460	0.82↓
4th frequency (Hz)	8.440	8.424	8.407	8.391	2.52↓

Table 4 summarizes the evolution of Models 1 and 2 and the Updated Model, including the numerical model (f_{NM}) and experimental natural frequencies obtained with the CFDD method (f_{CFDD}), as well as the MAC index of the updated numerical model.

Table 4. Model Evolution – Comparison Between the Natural Frequencies and Mode Shapes In The Mu Process

Mode	fCFDD (Hz)	Model 1	Model 2	Updated Model		
		fNM (Hz)	fNM (Hz)	fNM (Hz)	FER (%)	MAC
1st	1.617	1.640	1.635	1.617	0.00	0.9994
2nd	3.288	3.242	3.242	3.234	1.64↓	0.9975
3rd	5.505	5.447	5.447	5.460	0.82↓	0.9373
4th	8.608	8.344	8.341	8.391	2.52↓	0.9744

The initial model (Model 1) provided a good correlation between the numerical and experimental dynamic properties (natural frequencies and mode shapes). The FER index was 1.42% for the first natural frequency and had a maximum value of 3.07% for the fourth natural frequency. The manual updating process sought to maximize the index reduction for the first mode shape, which was successfully achieved (FER = 0.00%), combined with a maximum reduction in the difference from 3.07% to 2.52%. The final model (Updated Model) also provided a good correlation between the mode shapes; the lowest value obtained for the MAC index was 0.9373 for the third mode shape. Figure 12 shows the first four flexural mode shapes of the Updated Model.

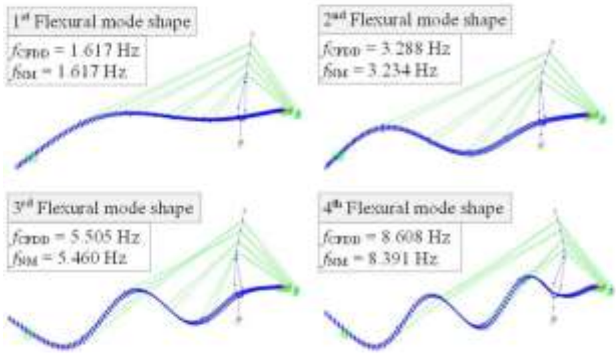

Fig. 12. Mode shapes of the Updated Model

V. CONCLUSIONS

The numerical modelling and calibration of a cable-stayed footbridge based on experimental dynamic properties and simplified approaches were discussed in this paper. The dynamic identification step, and the modelling of cablestayed structures and their fitting to dynamic properties presented the following characteristics:

- At least four natural frequencies, in the 0–24 Hz frequency range, were identified in all stay cable tests. These were used to determine the cable forces on-site. The procedure was effective because the deck shape obtained with the numerical model resembled that observed visually on-site and was directly dependent on the set forces of the stay cables. However, despite the apparent success, future studies should evaluate the stay forces on-site considering the actual boundary conditions of the element;
- In the global structure tests, the data acquisition system and identification methods (CFDD and SSI-UPC) were excellent tools for obtaining the first four flexural mode shapes within the 0–9 Hz frequency range. Both methods resulted in very similar natural frequency values, with a maximum difference of 0.133 Hz (2.42%). The CFDD method was chosen for the MU process based on qualitative analysis of the experimental mode shapes.
- A simplified 3D FE model composed of 3D beam elements with equivalent stiffness could adequately represent the dynamic behaviour of the footbridge, exhibiting good correlation with the experimental natural frequencies and mode shapes. The initial model was already able to provide a good correlation with the experimental natural frequencies and mode shapes, with a FER index of 1.42% for the first natural frequency and a maximum FER of 3.07% for the fourth natural frequency. Additionally, the applied nonlinear static analysis was important for providing the real stiffness and geometry of the deformed-shape footbridge model. Thus, the modal analysis considered the cable forces and the structure deformability, which are important characteristics of cable-stayed structures;
- Two tools implemented in SAP2000 were used. The first tool considers the stay cables as "catenary elements", providing the deformed shape of the cable due to its

selfweight, axial force, and length. This leads directly to the second-order effect caused by the cable self-weight, consequently defining the cable stiffness. In the literature, compared with the various modelling approaches that have achieved varying degrees of success, this model seems to be more realistic. The second tool, called "Target Force," was used to impose the cable axial forces identified on-site. These two issues helped in the MU process, since Model 1 has already provided good correlation with the experimental model;

- In this case, the springs affected only the first identified mode shape, and a single adjustment of the boundary conditions, represented by the introduction of translational and rotational springs, was sufficient to generate Model 2, which was used in the sensitivity analysis. Thus, the boundary conditions were not included in the sensitivity analysis;
- The sensitivity analysis based on a 5% increase in the selected structural properties was an effective and practical option to direct the manual tuning as the possible variation of the elastic modulus of the stay cable steel is in the range of ± 5%;
- Although it is a simpler approach, the manual MU process was efficient for producing a numerical model with an excellent approximation of the dynamic behaviour of the footbridge obtained on-site. Both the FER and MAC index values were considered very good, with a maximum FER of 2.52% for the fourth natural frequency and minimum MAC value of 0.9373 for the third mode shape. These results indicate the ability of the model to be used for SHM.

ACKNOWLEDGMENT
The authors would like to acknowledge DNIT for authorizing the tests, A. Araujo and E. Nunes for their assistance during the tests, and the State University of Santa Cruz for financial support.

REFERENCES

1. Asadollahi, P., Huang, Y., and Li, J. 2018. Bayesian finite element model updating and assessment of cable-stayed bridges using wireless sensor data. Sensors. 18 (Sep. 2018), 1-22.
2. Bedon, C., Dilena, M., and Morassi, A. 2016. Ambient vibration testing and structural identification of a cable-stayed bridge. Meccanica. 51 (Apr. 2016), 2777-2796.
3. Benedettini, F., and Gentile, C. 2011. Operational modal testing and FE model tuning of a cablestayed bridge. Engineering Structures. 33 (Jun. 2011), 2063-2073.
4. Bin, Z., Weiping, X., and Jian, X. 2011. Nonlinear Analysis for the Lateral Vibration of Footbridges Induced by Pedestrians. Journal of Bridge Engineering. 18 (Sep. 2011): 122-130.
5. Brownjohn, J. M. W., Bocian, M., Hester, D.,
6. Quattrone, A., Hudson, W., Moore, D., Goh, S., and Lim, M. S. 2016. Footbridge system identification using wireless inertial measurements units for force and response measurements. Journal of Sound Vibration. 384 (Dec. 2016), 339-355.
7. Bursi, O. S., Kumar, A., Abbiati, G., and Ceravolo, R. 2014. Identification, model updating and validation of a steel twin deck curved cable-stayed footbridge. Computer-Aided Civil and
8. Infrastructure Engineering. 29 (Oct. 2014), 703722.
9. Chisari, C., Bedon, C., and Amadio, C. 2015. Dynamic and static identification of base-isolated bridges using genetic algorithms. Engineering Structures. 102 (Nov. 2015), 80-92.
10. Cismaşiu, C., Narciso, A. C., and dos Santos F. P. A. 2014. Experimental Dynamic Characterization and Finite-Element Updating of a Footbridge Structure. Journal of Performance of Constructed Facilities. 29 (Apr. 2014), 1-29.
11. Daniell, W. E., and Macdonald, J. H. G. 2007. Improved finite element modelling of a cablestayed bridge through systematic manual tuning. Engineering Structures. 29 (Mar. 2007), 358-371.
12. Deng, Z., Huang, M., Wan, N., and Zhang, J. 2023. The Current Development of Structural Health Monitoring for Bridges: A Review. Buildings. 13 (May 2023), 1360.
13. Güemes, A., Fernandez-Lopez A., Pozo A.R., and Sierra-Pérez, J. 2020. Structural Health Monitoring for Advanced Composite Structures: A Review. Journal of Composites Science. 4 (Jan. 2020), 13.
14. Feng, P., Wang, Z., Jin, F., and Zhu, S. 2019. Vibration Serviceability Assessment of Pedestrian Bridges Based on Comfort Level. J. Perform. Constr. Facil. 33 (Jun. 2019), 04019046.
15. Jacobsen, N.-J., Andersen, P., and Brincker, R. 2008. Applications of frequency domain curvefitting in the EFDD technique. In Proceedings of the 26th IMAC, A Conference and Exposition on Structural Dynamics.
16. Jacobsen, N.-J., and Andersen, P. 2008. Curvefitted enhanced frequency domain decomposition – A robust technique to harmonic excitation in operational modal analysis. In Proceedings of the 15th International Congress on Sound and Vibration (ICSV 15).
17. Malekjafarian, A., and Obrien, E. J. 2014. Identification of bridge mode shapes using short time frequency domain decomposition of the responses measured in a passing vehicle. Engineering Structures. 81 (Dec. 2014), 386-397.
18. Mishra, M., Lourenço, P. B., and Ramana, G. V. 2022. Structural health monitoring of civil engineering structures by using the internet of things: A review. Journal of Building Engineering. 48 (May 2022), 103954.
19. Nimmen, K. V., Verbeke, P., Lombaert, G., De Roeck G., and den Broeck, P. V. 2016. Numerical and Experimental Evaluation of the Dynamic Performance of a Footbridge with Tuned Mass Dampers. Journal of Bridge Engineering. 21 (Jan. 2016), C4016001.

20. Nunes, D de S., Brito, J. L. V., and Doz, G. N. 2019. A low-cost data acquisition system for dynamic structural identification. IEEE Instrumentation & Measurement Magazine. 22 (Oct. 2019), 64-72.
21. Nunes, D de S., Brito, J. L. V., and Doz, G. N. 2023. Dynamic identification of a cable-stayed footbridge using a low-cost data acquisition system. IBRACON Structures and Materials Journal, 16 (Apr. 2023), e16610.
22. Park, W., Park, J. Y., and Kim, H.-K. 2014. Candidate model construction of a cable-stayed bridge using parameterised sensitivity-based finite element model updating. Structure and
23. Infrastructure Engineering. 11 (Jul. 2014), 11631177.
24. Peeters, B., and De Roeck, G. 1999. Referencebased stochastic subspace identification for outputonly modal analysis. Mech. Syst. Sig. Process. 13 (Nov. 1999), 855-878.
25. Peeters, B. 2000. System identification and damage detection in civil engineering. Ph.D. Thesis, Faculty of Applied Sciences, Civil Engineering Department, Catholic University of Leuven.
26. Ren, W.-X., and Chen, H.-B. 2010. Finite element model updating in structural dynamics by using the response surface method. Engineering Structures. 32 (Aug. 2010), 2455-2465.
27. Schlune, H., Plos, M., and Gylltoft, K. 2009. Improved bridge evaluation through finite element model updating using static and dynamic measurements. Engineering Structures. 31 (Jul.), 1477-1485.
28. Setareh, M. 2016. Vibration Serviceability Issues of
29. Slender Footbridges. Journal of Bridge
30. Engineering. 21 (Jun. 2016), 04016084.
31. Setareh, M., and Gan, S. 2018. Vibration Testing, Analysis, and Human-Structure Interaction Studies of a Slender Footbridge. Journal of Performance of Constructed Facilities. 32 (Jul. 2018), 04018068.
32. Sharry, T., Guan, H., Nguyen, A., Oh, E., and Hoang, N. 2022. Latest Advances in Finite Element Modelling and Model Updating of Cable-Stayed Bridges. Infrastructures. 7 (Jan. 2022), 8.
33. Sun, L., Shang, Z., Xia, Y., Bhowmick, S., and Nagarajaiah, S. 2020. Review of Bridge Structural Health Monitoring Aided by Big Data and Artificial Intelligence: From Condition Assessment to Damage Detection. Journal of Structural Engineering. 146 (Mar. 2020), 04020073.
34. Svendsen, B.T., Petersen, Ø.W., Frøseth, G.T., and Rønnquist, A. 2021. Improved finite element model updating of a full-scale steel bridge using sensitivity analysis. Structure and Infrastructure Engineering. 19 (Jul. 2021), 315-331.
35. Tubino, F., Carassale, L., and Piccardo, G. 2016. Human-Induced Vibrations on Two Lively Footbridges in Milan. Journal of Bridge Engineering. 21 (Jan. 2016), C4015002.
36. Wu, J. R., and Li, Q. S. 2004. Finite element model updating for a high-rise structure based on ambient vibration measurements. Engineering Structures. 26 (Jun. 2004), 979-990.
37. Yue, L., and Li, S. 2014. The finite element model updating of long span cable-stayed bridge based on static and dynamic loading test. Applied Mechanics and Materials. 644-650 (Sep. 2014), 5014-5018.
38. Zhu, Q., Y. L. Xu, and X. Xiao. 2014. Multiscale modeling and model updating of a cable-stayed bridge. I: Modeling and influence line analysis. Journal of Bridge Engineering. 20 (Nov. 2014), 04014112.